Polarized-neutron-reflectivity confirmation of 90° magnetic structure in Fe/Cr(001) superlattices

S. Adenwalla, G. P. Felcher, Eric E. Fullerton, and S. D. Bader

Materials Science Division, Argonne National Laboratory, Argonne, Illinois 60439

Polarized-neutron reflectivity together with magnetization and magnetotransport measurements on a (001)-oriented [Fe(14 Å)/Cr(74 Å)]$_{20}$ superlattice confirms the existence of 90° alignment of adjacent Fe layers due to biquadratic interlayer coupling. Each Fe layer is in a single domain state and the magnetic structure is coherent throughout the layered stack. The biquadratic coupling, however, is suppressed below the Cr Néel temperature ($T_N=187$ K) as the Fe layers uncouple. But by field cooling through T_N it is possible to retain a metastable biquadratic arrangement.

I. INTRODUCTION

Ferromagnetic films separated by nonferromagnetic spacers can exhibit an oscillatory exchange coupling between the ferromagnetic layers as a function of spacer thickness.[1,2] Two oscillatory periods have been observed in Fe/Cr samples:[3,4] a "long" 18-Å period which is independent of crystallographic orientation of the spacer, and a "short" 2.1-monolayers (ML) period along the $\langle 100 \rangle$ which results from the nested feature of the Cr Fermi surface and which is responsible for the spin-density-wave antiferromagnetism of Cr. The interlayer coupling energy is of the form $J_1 \mathbf{m}_1 \cdot \mathbf{m}_2$, where J_1 is the bilinear coupling constant and $\mathbf{m}_1$ and $\mathbf{m}_2$ are the magnetizations of two adjacent ferromagnetic layers. The coupling energy is minimized when $\mathbf{m}_1$ and $\mathbf{m}_2$ are parallel or antiparallel to each other depending on whether J_1 is positive or negative, respectively. It was discovered in Fe/Cr/Fe(001) trilayers that 90° alignment of the Fe layers occurs in narrow transition regions, where J_1 is small, located between the dominant antiferromagnetic (AFM) and ferromagnetic (FM) coupled regions.[6] An additional phenomenological term $J_2(\mathbf{m}_1 \cdot \mathbf{m}_2)^2$ can be included to describe the 90° coupling, where J_2 is referred to as the biquadratic coupling constant. For $J_2 < 0$ the energy is minimized for $\mathbf{m}_1$ perpendicular to $\mathbf{m}_2$. Biquadratic coupling has since been observed in a number of trilayer [e.g., Fe/Cr/Fe,[3,6] Fe/Al/Fe,[7] Fe/Cu/Fe,[8] Fe/Ag/Fe,[8,9] and Fe/Au/Fe (Ref. 10)] and superlattice [e.g., FeNi/Ag (Ref. 11) and Fe/Cr (Ref. 12)] structures. Also, the temperature dependence[8-11] of J_2, in general, has been shown experimentally to be stronger than that of J_1.

The origin of the biquadratic coupling has been attributed either to intrinsic properties of the spacer layer[13] or to extrinsic factors such as (i) dipolar fields resulting from rough interfaces,[14] (ii) superparamagnetic impurities within the spacer ("loose spins"),[15] or (iii) fluctuations in the spacer thickness which average out the short-period oscillations.[15,16] Recent experiments on Fe/Cr(001) superlattices identified the Néel transition for Cr spacers >42 Å thick.[17] It was also reported that the magnetic properties of superlattices with such relatively thick Cr spacers are dramatically altered at the Néel temperature (T_N). For $T > T_N$, the magnetic properties are consistent with 90° coupling of adjacent Fe layers, while for $T < T_N$ the layers uncouple. In the present paper we use polarized-neutron reflection combined with magnetiza-tion and magnetotransport to study the biquadratic coupling of an [Fe(14 Å)/Cr(74 Å)]$_{20}$ superlattice near T_N of the Cr spacer. The neutron results confirm both the 90° alignment of the Fe layers for $T > T_N$, and that the sample is in a single-domain state over an area of order of a cm^2. For $T < T_N$, the biquadratic coupling is suppressed and the magnetic configuration of the Fe layers depends sensitively on the applied field in which the sample is cooled through T_N.

The (001)-oriented [Fe(14 Å)/Cr(74 Å)]$_{20}$ was epitaxially grown by dc magnetron sputtering onto a 2.5×2.5 cm^2 MgO(001) single-crystal substrate. A 100-Å Cr(001) base layer was deposited at 600 °C onto the MgO prior to the superlattice growth, which occurred at 75 °C. The epitaxial relationship is Fe/Cr [100]‖MgO[100]. At this thickness of Cr the bilinear coupling constant is small[5] and, as will be shown, the biquadratic coupling is dominant. Transport and magnetization measurements were made on a 3×10 mm^2 section cleaved from the substrate. Measurements were made with the applied field H along either the Fe[100] easy axis or the [110] hard axis. The magnetization measurements utilized a superconducting quantum interference device (SQUID) magnetometer at temperatures between 10 and 350 K. Transport was measured using a standard, four-terminal dc technique with a constant current source. The neutron measurements were performed at the POSY1 beamline at Argonne's Intense Pulsed Neutron Source.

II. RESULTS

A. Measurement of T_N

Transport measurements are often used to identify the Néel transition in Cr and Cr alloys.[18,19] The resistivity (ρ) is enhanced above its extrapolated value as T decreases through T_N. This increase in ρ is the result of energy gaps opening on the nested parts of the Fermi surface and is high-est when the current is parallel to the nesting vector $\mathbf{Q}$.[18] Shown in Fig. 1 is ρ vs T measured at 1 kOe. In this field, the Fe layers are aligned parallel to H and there are no additional magnetoresistance (MR) contributions to ρ due to misalign-ment of the Fe layers. An anomaly in ρ appears in Fig. 1 as an increase above its expected linear behavior shown by the dashed-line extrapolation. The $\approx 10\%$ enhancement of ρ at T_N is consistent with values reported for bulk Cr and Cr films. The resistive transition is, however, considerably
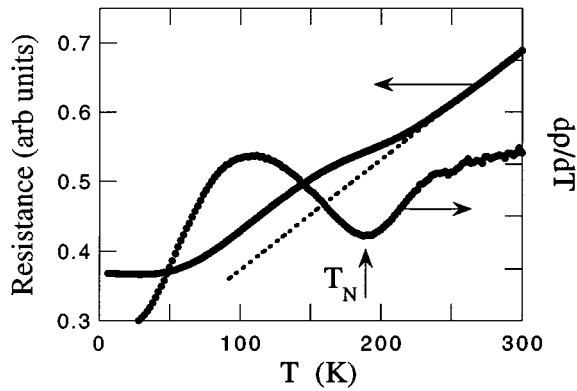
FIG. 1. Resistance measurements on the $[\text{Fe}(14\ \text{Å})/\text{Cr}(74\ \text{Å})]_{20}$ superlattice showing the Néel transition of the Cr. T_N is defined as the point of inflection of the $d\rho/dT$ curve.

broader than that of single-crystal Cr in which a singularity in ρ is observed at T_N. For such broad transitions, T_N is often defined as the point of inflection in the ρ-vs-T curve which can be identified as a minimum in $d\rho/dT$. Using this criterion, T_N for the present sample is 187 ± 5 K.

B. Magnetization and magnetoresistance

Magnetization and magnetotransport measurements are shown in Figs. 2 and 3, respectively, with H in-plane along both the Fe [100] easy and [110] hard axes. The figures show the first-quadrant hysteresis loops in decreasing field. At high fields, the magnetic moments are aligned with the field at the
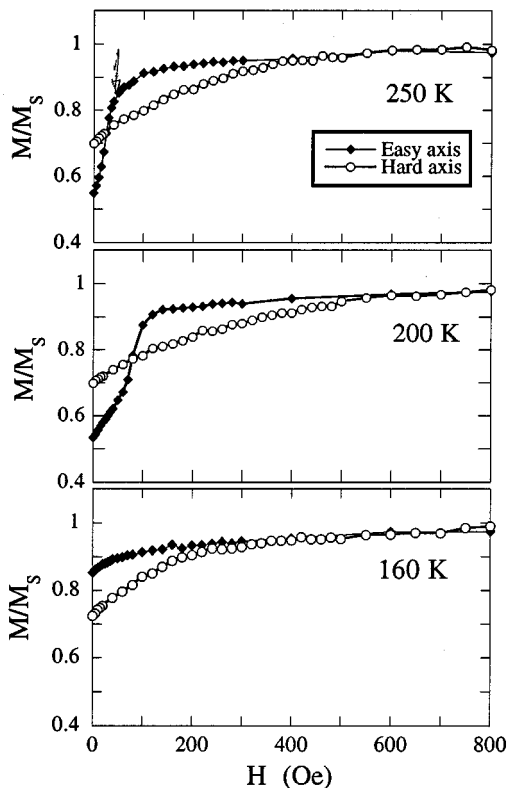

FIG. 2. Upper quadrant of the magnetization along the easy [100] orientation and hard [110] orientations. Arrows indicate easy-axis saturation fields H_s.
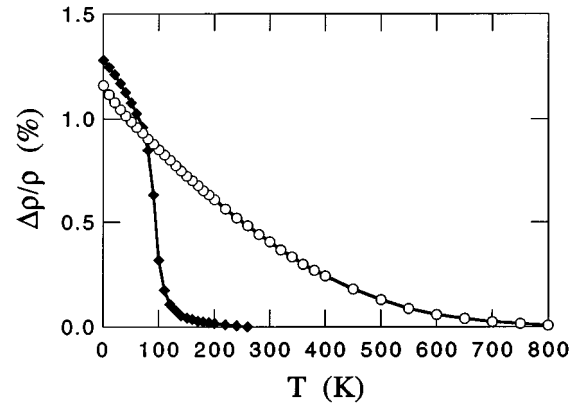

FIG. 3. Magnetoresistance with H applied along easy and hard axes.

saturation value M_s. As H decreases, the hard-axis magnetization gradually decreases to its remanent value $M_r\approx0.7M_S$ for all temperatures. This behavior is consistent with coherent rotation of the Fe layers toward the easy axis and as expected $M_r=1/\sqrt{2}M_s$. For $T>T_N$, the easy-axis magnetization decreases sharply at low fields to $M_r\approx0.54M_s$. This suggests biquadratic coupling of the Fe layers in which alternate layers are sequentially magnetized parallel or perpendicular to the field. (The slightly higher M_r value from the expected $0.5M_s$ is due to the coercivity of the Fe layers.) The 90° alignment of the Fe layers at low fields gives the expected enhanced MR as seen in Fig. 3. The shape of both the magnetization and magnetoresistance are consistent with a combination of biquadratic coupling and cubic anisotropy. Below T_N, there is a dramatic change in the magnetization loops, as reported previously.[17] M_r increases along the easy axis, and the saturation field along the hard axis decreases, which both suggest that the biquadratic coupling is suppressed.

The temperature dependence of the saturation MR value (denoted $\Delta\rho/\rho$) and the saturation field H_s are shown in Fig. 4. H_s is defined as the field at which the sharp drop in the easy-axis magnetization [see arrows in Fig. 2] and rise in the MR occur. Both $\Delta\rho/\rho$ and H_s are strongly temperature dependent and show anomalies at the measured value of T_N consistent with previous measurements. H_s exhibits a maximum at 205 K and goes to zero just below T_N. The MR exhibits an anomaly at T_N consistent with the suppression of the biquadratic coupling.

C. Neutron reflectivity measurements

The neutron reflectivity was measured at 300, 205, 160, and 20 K. We focus primarily on the 205- and 160-K results because they straddle T_N. At 205 K, the biquadratic coupling is strongest (as evidenced from the magnetization measurements) and measurements taken at two applied fields, 6 and 40 Oe, both show evidence of a 90° coupling; in addition we see the effect of the Zeeman energy term as the moments cant towards the applied field. The arrangement of POSY1 permits the reflectivity to be measured with and without polarization analysis. A polarized beam of neutrons passes through a flipper which is turned on at every alternate pulse. This allows us to measure the reflectivity of the sample for
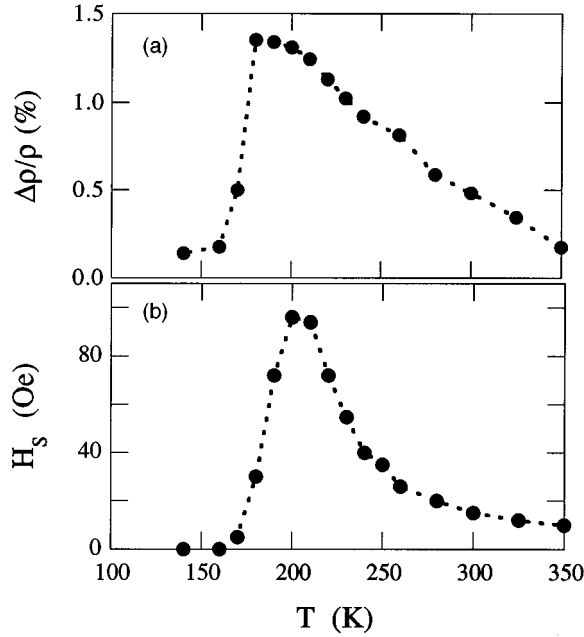
FIG. 4. (a) Saturation magnetoresistance $\Delta\rho/\rho$ and (b) saturation field H_s measured as a function of temperature.

initial polarizations of the beam either parallel or antiparallel to H as given by R^+ and R^-, respectively. An analyzer placed in the path of the reflected neutron beam reflects neutrons of only one polarization (+). Using this analyzer we can measure the non-spin-flip (NSF) reflectivity R^{++} and the spin-flip (SF) reflectivity R^{-+}. The relation between these quantities is given by

$$R^+=R^{++}+R^{+-},$$

$$R^-=R^{--}+R^{-+},$$

and

$$R^{-+}=R^{+-}.$$

The NSF reflectivities R^{++} and R^{--} depend upon both the nuclear scattering potential bN and the component of the magnetization parallel (or antiparallel) to the neutron spin. Hence, the NSF reflectivity is nonzero even in the absence of magnetization, and the difference between R^{++} and R^{--} is a measure of the component of the sample magnetization parallel to H. In contrast the SF contribution arises *solely* from the perpendicular component of the magnetization and is zero if this component is not present. Neutron reflectivity with polarization analysis is hence an ideal probe for studying the magnetization profile of a multilayer system.

Shown in Fig. 5 are reflectivity results measured at 205 K with $H=40$ Oe along the easy axis. The measurements were taken over a range of momenta $k=2\pi\sin\theta/\lambda$ (where θ is the angle of incidence of the neutrons on the surface, and λ is the neutron wavelength) from the region of total external reflection through the first superlattice Bragg reflection at $k=0.037$ Å^{-1}. To check on the magnetic-history dependence of the sample, data were taken while cooling the sample from room temperature in either the full field (3.5 kOe) or in low field (6 Oe). The results for $T>T_N$ were identical. The spectrum in
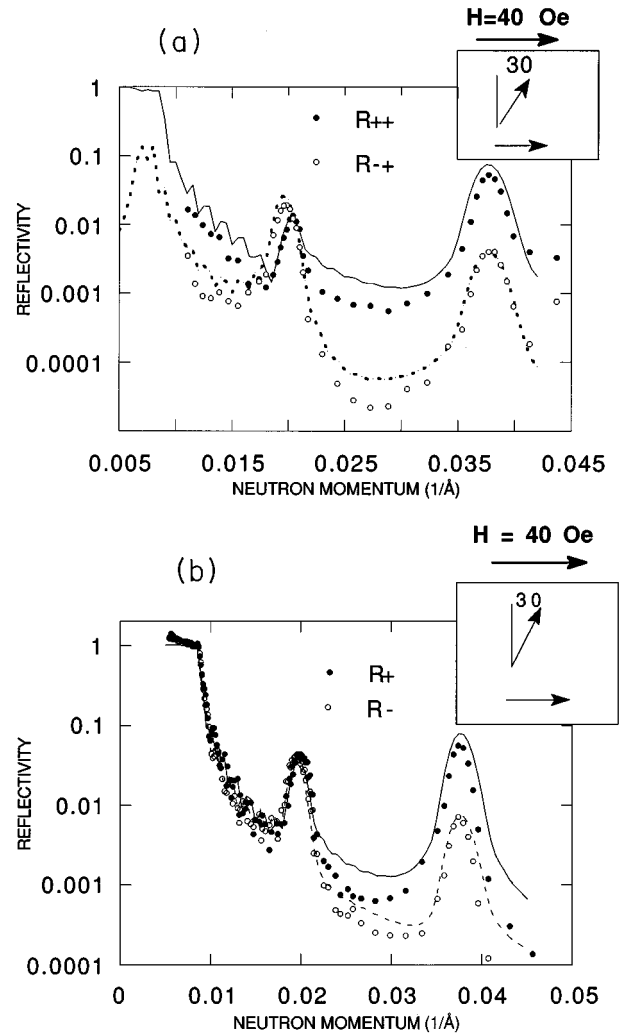

FIG. 5. Neutron reflectivity measured with (R^{++} and R^{-+}) and without (R^+ and R^-) polarization analysis along the easy [100] axis at $H=40$ Oe and $T=205$ K. The lines are the fit to the data for the spin structure shown in the inset.

Fig. 5 consists of two Bragg peaks and higher-frequency Kiessig oscillations resulting from the finite size of the superlattice. The peak at high k, the ferromagnetic (FM) peak, corresponds to the superlattice periodicity and results from both the nuclear scattering from the layers and components of the Fe-layer magnetization ferromagnetically aligned with H. The peak at low k, the antiferromagnetic (AFM) peak, results from the noncollinear alignment of the Fe layers and corresponds to a doubling of the magnetic unit cell. Both peaks are present for all four reflectivity curves: R^+, R^-, R^{++}, and R^{-+}.

There are a number of striking features in the data. The presence of an AFM peak in the SF reflectivity indicates that there is a perpendicular component of magnetization with a repeat distance of twice the superlattice spacing; this is a signature of the presence of interlayer coupling. The width of the AFM peak indicates that the magnetic structure is coherent throughout the thickness of the superlattice. The R^+ and R^- AFM peaks are shifted with respect to each other, the R^- peak being shifted to lower k [as can be seen more clearly in Fig. 6]. We fitted the reflectivity data in the conventional
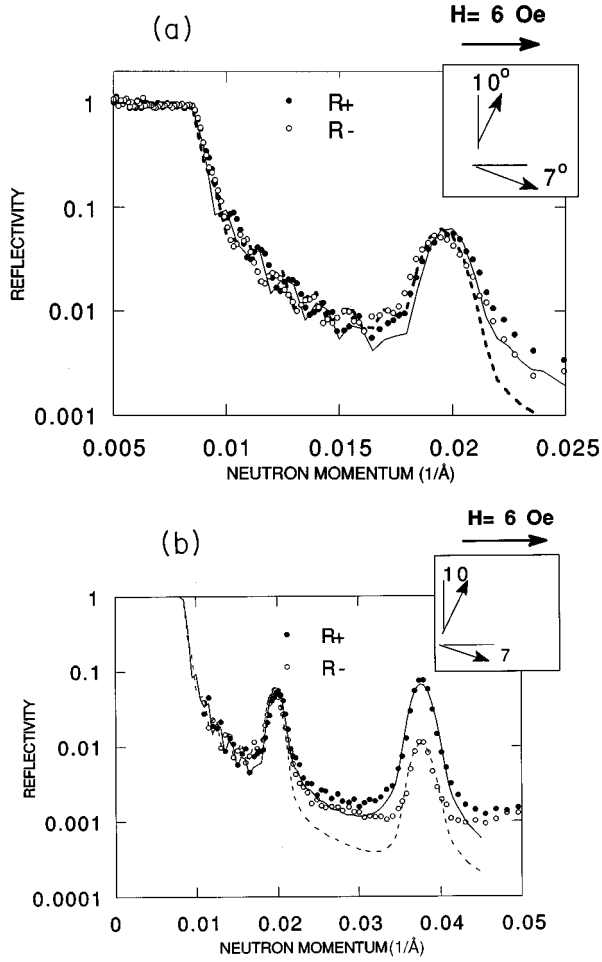
(a)   H= 6 Oe

(b)   H= 6 Oe

FIG. 6. Neutron reflectivity measured without polarization analysis along the easy [100] axis at $H=6$ Oe and $T=205$ K. The lines are the fit to the data for the spin structure shown in the inset. (a) low-k data showing clearly the splitting of the AFM peak; (b) high-k data.

manner by assigning a refractive index to each layer, matching boundary conditions and then calculating the total reflectivity. The only parameters in the fit were the direction of magnetization in each layer; the thickness was known from earlier x-ray measurements and the scattering-length density was assumed to be that of the bulk. We assume a two-sublattice model in which the angle of magnetization of each sublattice with respect to H is a fitting parameter.

The solid lines in Fig. 5 represent fits to the data, and the resultant magnetic structures are shown in the inset. (Note that all magnetizations are in-plane: parallel and perpendicular refer to in-plane directions with respect to H). The tilt away from the 90° arrangement is due to the Zeeman energy, which makes it energetically favorable for the magnetization to cant towards the field direction. Measurements at lower fields show a substantial decrease in the tilt [see Fig. 6]. The separation of the AFM peak is successfully modeled assuming a single-domain sample; this results in the the reflectivity being slightly weighted in favor of the front face of the sample due to attenuation of the neutron beam as it traverses the sample. (This weighting effect would be obscured in a multidomain sample.) In the case shown, the shift of the AFM peak indicates that the top Fe layer is magnetized perpendicular to H.

TABLE I. Normalized intensities of the ferromagnetic and antiferromagnetic peaks for the various reflectivities shown in Fig. 5.

	I^+	I^-	I^{++}	I^{-+}
AFM	1.213	1.103	0.408	0.802
FM	7.45	0.915	6.87	0.582

An alternative method for a generalized fitting of the reflectivity data is to analyze the peak intensity within the framework of the conventional kinematic theory, as is often done in large-angle diffraction. Any two-sublattice magnetic structure can be resolved into FM and AFM components: the FM component being along the magnetization axis and the AFM component lying perpendicular to it. A similar method was used to fit the FM peak in the experiments on NiFe/Ag multilayers by Rodmacq et al.[11] For example, a biquadratic structure with spins exactly at 0° and 90° could be resolved into an FM component (repeated every lattice spacing) at 45° and an AFM component (which alternates its direction at sequential layers, i.e., having a double repeat distance) at 135° to H. In this case, both components have the same magnitude. In general, the intensities of the AFM and FM peaks for the SF and NSF reflectivities are proportional to

$$I_{FM}^+ \propto (\mathbf{n}+\mathbf{f}_p)^2+\mathbf{f}_s^2, \quad I_{FM}^- \propto (\mathbf{n}-\mathbf{f}_p)^2+\mathbf{f}_s^2, \quad (1a)$$

$$I_{FM}^{++} \propto (\mathbf{n}+\mathbf{f}_p)^2, \quad I_{FM}^{-+} \propto \mathbf{f}_s^2, \quad (1b)$$

$$I_{AFM}^+ \propto \mathbf{a}_p^2+\mathbf{a}_s^2, \quad I_{AFM}^- \propto \mathbf{a}_p^2+\mathbf{a}_s^2, \quad (2a)$$

$$I_{AFM}^{++} \propto \mathbf{a}_p^2, \quad I_{AFM}^{-+} \propto \mathbf{a}_s^2, \quad (2b)$$

where $\mathbf{n}$ is the nuclear scattering amplitude $[(bN)_{Fe} - (bN)_{Cr}]$, $\mathbf{f}$ and $\mathbf{a}$ denote the FM and AFM components, respectively, and the subscripts s and p refer to magnetization parallel and perpendicular to the neutron spin (and H), respectively. The values for these intensities obtained from the data in Fig. 5 at 205 K and 40 Oe are given in Table I. The values are in units of 10^{-8} Å^2/atom obtained after renormalizing the experimental intensities.
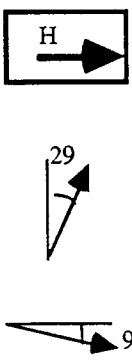
The magnitude of the AFM and FM components, and the angle they make with the magnetic field are calculated with the aid of Eqs. (1) and (2) and presented in Table II. By inserting the correct values for $\mathbf{n}$ in Eqs. 1(a) and 1(b) [here $n=5\times10^{-6}$ Å^{-1}, from the bulk values for Fe and Cr] we obtain the magnitude of the FM component. Fitting the AFM

TABLE II. Amplitude and orientation of the ferromagnetic and antiferromagnetic component with reference to the applied field (40 Oe).

	Magnitude (μ_B)	Angle (with respect to field)
AFM	0.85	55°
FM	1.72	35°

TABLE III. Amplitude and orientation of the sublattice magnetization in reference to the applied field (40 Oe).

	Magnitude	Orientation	
			H →
Sublattice I	1.93	61°	29
Sublattice II	1.93	-9°	9

peak yields the magnitude of the AFM component. The ratio between I^{++} and I^{-+} gives the orientation of the components. Notice that the AFM and FM components are at 90° to each other, satisfying the condition *necessary* for the validity of any model consisting of two sublattices with magnetization of the same size but oriented in different directions. If that model is accepted, the sublattice magnetizations have the values calculated in Table III. With these results one can reconstruct the spin structure of the sample, which yields one similar (within ±10°) to that obtained from direct fitting of the reflectivity data. The discrepancy between the two methods is due to the fact that the two-sublattice method has error bars of up to 5° in the absolute orientation of the moments (although the error bar for the relative orientation is very small).

Hard-axis measurements (with polarization analysis) at the same temperature (205 K) and field (40 Oe) show that the AFM peak arises solely from spin-flip scattering, as would be expected for a configuration in which the moments of sequential layers are alternatively aligned symmetrically about H. There is no splitting between the R^+ and R^- AFM peaks, since $R^{+-}=R^{-+}$. Fitting the reflectivity and polarization data we find that the maoments are aligned at +45° and −45° to the field.

TABLE IV. Amplitude and orientation of the sublattice magnetizations with reference to the applied field (6 Oe).

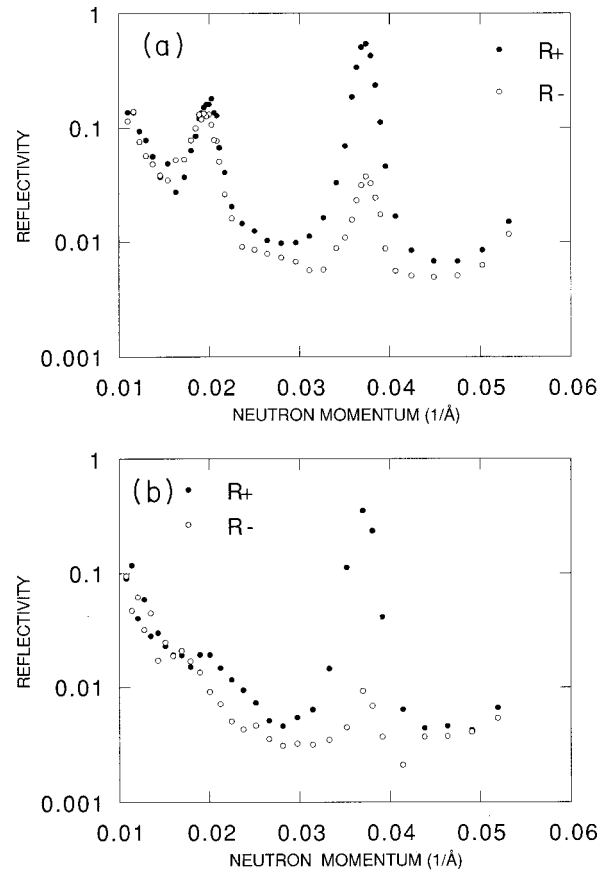|	Magnitude	Orientation	
			H →
Sublattice I	2.0	70°	20
Sublattice II	2.0	-2°	2

FIG. 7. Neutron reflectivity measured without polarization analysis along the easy [100] axis at $T=160$ K. (a) Field cooled in 6 Oe showing the presence of the AFM peak and (b) data taken after saturating the sample in a field of 3.5 kOe in which the AFM peak is absent.

Decreasing the field to 6 Oe decreases the tilt from about 30° to between 10° and 20°, as would be expected, but the basic structure remains the same. The fit to the data and the spin structure are shown in Figs. 6(a) and 6(b). Table IV gives the magnitudes and orientations of the two sublattice magnetizations and the spin structure obtained from the analysis of the peak intensities.

The orthogonality of the AFM and FM components is a condition necessary for the validity of a two-sublattice model, but is by no means sufficient. The same diffracted intensities could, in principle,[21] be obtained from a sample made of FM and AFM domains as in the two-axis structure proposed here. However, this holds only in the limit of the kinematic approximation. Close to the critical edge the deviation of the neutron momentum in the material (compared to the vacuum value) provides additional information. Figure 6 shows the low-momentum reflectivities $R^+=R^{++}+R^{+-}$ and $R^-=R^{--}+R^{-+}$. The low-k oscillations are due to the interference of neutron waves reflected from the surface and the substrate; these "total thickness oscillations" occur in the region of momenta where all details of the superlattice are averaged out. For the two neutron spin states + and − the reflectivity minima occur at different k values. If the system is homogeneous[20]

$$(k^+)^2 = k_0^2 - (4\pi bN + cB),$$

$$(k^-)^2 = k_0^2 - (4\pi bN - cB),$$

and $\Delta k = 2B/k$, where B is (in proper units) the magnetic induction of the bulk sample. From Fig. 6 it can be seen that the overall magnetization of the sample is well fitted as being biquadratically coupled. If, instead, the system was composed of AFM and FM domains, the displacement Δk would have been larger due to the larger net magnetization of the sample. But, then there would have been damped oscillations (due to the fact that the AFM coupled portions of the sample would have zero net magnetization and, hence, would not contribute to the shifted oscillations).

D. Temperature dependence of the coupling

The behavior of the system as temperature is lowered below 205 K depends strongly on the magnetic-field history. Data at 160 K were collected in three different ways. Initially the sample was cooled in a magnetic field of 40 Oe from 205 K. This produced a structure in which the AFM peak is extremely small, indicating that the sample is almost completely FM aligned. If, however, the sample is cooled below 205 K in a low field (6 Oe), the AFM peak is still present, albeit at a slightly lower intensity [Fig. 7(a)]. The peak width is the same, and the splitting of the R^+ and R^- AFM peaks indicates that the sample is still in a single-domain state. The slightly diminished intensity of these peaks is due to the decrease in the spin-flip reflectivity, which can be attributed to a tilt of the perpendicular spins toward H. A third measurement was made after saturating the sample from 6 Oe to a field of 3.5 kOe at 160 K and then reducing the field back to 6 Oe, which is comparable to the conditions under which the magnetization measurements were made. In agreement with the square hysteresis loop, this showed a complete absence of the AFM peak [Fig. 7(a)]. The FM peak did not change in peak width, intensity, or polarization. This result suggests that at 160 K, the layers are truly uncoupled. When the spins are in a 90° alignment, each Fe layer is along a crystallographic easy axis. When cooled below T_N in a field below the coercive field ($H_c \approx 15$ Oe) of the Fe layers, the Fe layers remain in this metastable configuration. Applying a modest field ($H > H_c$) aligns the layers and the system cannot get back to the 90° configuration without warming above T_N.

III. CONCLUSIONS

We have studied the magnetic properties of an [FE(14 Å)/Cr(74 Å)]$_{20}$ superlattice above and below the Néel transition of the Cr layers. Resistivity measurements yield $T_N = 187$ K for this sample. For $T > T_N$, the Fe layers align alternately at nearly 0° and 90° with respect to an applied magnetic field, consistent with the presence of biquadratic coupling. The spins are tilted slightly away from the parallel and perpendicular positions due to the applied magnetic field. The 90° configuration is stable over a large sample area, and forms a coherent structure throughout the superlattice. Both neutron reflectivity and magnetization measurements are consistent with this picture. Proof of biquadratic coupling, as opposed to a combination of FM- and AFM-coupled domains, comes from the splitting of the AFM peak and the shift in the low-k oscillations in the neutron reflectivity. A simple analysis of the AFM and FM Bragg peaks shows that the results are well represented by a two spin system in which the AFM and FM components are at 90° to each other, thereby eliminating the possibility of inhomogeneities within the sample stacking arrangement. For temperatures just below T_N the Fe layers become uncoupled, but by cooling the sample through T_N in a small field, a metastable biquadratic arrangement can be stabilized. This work highlights the subtle interplay between the interlayer coupling of the Fe and the AF ordering of thick Cr spacers.

ACKNOWLEDGMENT

[1] P. Grünberg, R. Schreiber, Y. Pang, M. B. Brodsky, and C. H. Sowers, Phys. Rev. Lett. **57**, 2442 (1986).

[2] S. S. P. Parkin, N. More, and K. P. Roche, Phy. Rev. Lett. **64**, 2304 (1990).

[3] J. Ungaris, R. J. Celotta, and D. T. Pierce, Phys. Rev. Lett. **67**, 140 (1991).

[4] S. T. Purcell, W. Folkerts, M. T. Johnson, N. W. E. McGee, K. Jager, J. ann de Stegge, W. B. Zeper, W. Hoving, and P. Grünberg, Phys. Rev. Lett. **67**, 903 (1991).

[5] Eric E. Fullerton, M. J. Conover, J. E. Mattson, C. H. Sowers, and S. D. Bader, Phys. Rev. B **48**, 15 755 (1993).

[6] M. Ruhrig, R. Schaefer, A. Hubert, R. Mosler, J. A. Wolf, S. Demokritov, and P. Grünberg, Phys. Status Solidi A **125**, 635 (1991).

[7] C. J. Gutierrez, J. J. Krebs, M. E. Filipkowski, and G. A. Prinz, J. Magn. Magn. Mater. **116**, L305 (1992).

[8] Z. Celinski, B. Heinrich, and J. F. Cochran, J. Magn. Magn. Mater. **145**, L1 (1995).

[9] J. Ungaris, R. J. Celotta, and D. T. Pierce, J. Magn. Magn. Mater. **127**, 205 (1993).

[10] U. Rucker, S. Demokritov, E. Tsymbal, P. Grünberg, and W. Zinn, J. Appl. Phys. **78**, 387 (1995).

[11] B. Rodmacq, K. Dumesnil, P. Mangin, and M. Hennion, Phys. Rev. B **48**, 3556 (1993).

[12] A. Schreyer, J. F. Ankner, H. Zabel, M. Schafer, C. F. Majkrzak, and P. Grünberg, Physica B **198**, 173 (1994).

[13] For a general discussion, see K. B. Hathaway, in *Ultrathin Magnetic Structures II*, edited by B. Heinrich and J. A. C. Bland (Springer-Verlag, Berlin, 1994), pp. 45–81.

[14] S. Demokritov, E. Tsymbal, P. Gruneberg, W. Zinn, and I. K. Schuller, Phys. Rev. B **49**, 720 (1994).

[15] J. C. Slonczewski, J. Appl. Phys. **73**, 5957 (1993).

[16] J. C. Slonczewski, Phys. Rev. Lett. **67**, 3172 (1991).

[17] E. E. Fullerton, K. T. Riggs, C. H. Sowers, S. D. Bader, and A. Berger, Phys. Rev. Lett. **75**, 330 (1995).

[18] E. Fawcett, Rev. Mod. Phys. **60**, 209 (1988).

[19] E. Fawcett, H. L. Alberts, V. Yu. Galkin, D. R. Noakes, and J. V. Yakmi, Rev. Mod. Phys. **66**, 25 (1994).

[20] G. P. Felcher, R. O. Hilleke, R. K. Crawford, J. Haumann, R. Kleb, and G. Ostrowski, Rev. Sci. Instrum. **58**, 609 (1987).

[21] A. Schreyer, K. Bröhl, J. F. Ankner, C. F. Majkrzak, Th. Zeidler, P. Bödeker, N. Metoki, and H. Zabel, Phys. Rev. B **47**, 15 334 (1993).